

Journal of Materials Chemistry A

Accepted Manuscript

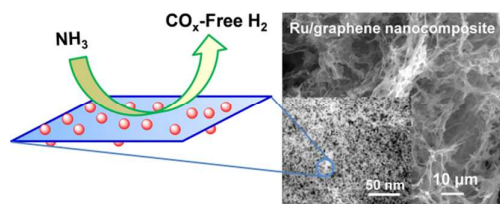


This is an *Accepted Manuscript*, which has been through the Royal Society of Chemistry peer review process and has been accepted for publication.

Accepted Manuscripts are published online shortly after acceptance, before technical editing, formatting and proof reading. Using this free service, authors can make their results available to the community, in citable form, before we publish the edited article. We will replace this *Accepted Manuscript* with the edited and formatted *Advance Article* as soon as it is available.

You can find more information about *Accepted Manuscripts* in the [Information for Authors](#).

Please note that technical editing may introduce minor changes to the text and/or graphics, which may alter content. The journal's standard [Terms & Conditions](#) and the [Ethical guidelines](#) still apply. In no event shall the Royal Society of Chemistry be held responsible for any errors or omissions in this *Accepted Manuscript* or any consequences arising from the use of any information it contains.



Support-dependent and structure-sensitive Ru supported by graphene showed an easily controllable nanoarchitecture, yielding drastically improved catalytic performance for ammonia decomposition.

Cite this: DOI: 10.1039/c0xx00000x

PAPER

www.rsc.org/xxxxxx

Graphene nanosheets supporting Ru nanoparticles with controlled nanoarchitectures form a high-performance catalyst for CO_x-free hydrogen production from ammonia

Gang Li,^{a,b} Hiroki Nagasawa,^b Masakoto Kanezashi,^b Tomohisa Yoshioka,^b and Toshinori Tsuru*^b

Received (in XXX, XXX) Xth XXXXXXXXXX 20XX, Accepted Xth XXXXXXXXXX 20XX

DOI: 10.1039/b000000x

To date, Ru is the most active single-metal catalyst known for ammonia decomposition, but its catalytic activity is support-dependent and structure-sensitive. Therefore, a unique support-anchored Ru nanoparticle with controllable size and morphology would be particularly important for high catalytic performance. In this work, we describe Ru nanoparticles supported by two-dimensional graphene nanosheets with a controlled nanoarchitecture that forms a novel composite catalyst that is capable of a high degree of ammonia decomposition. This high-quality Ru/graphene nanocomposite material was obtained *via* a cosolvent method (CS-Ru/graphene), in which ethylene glycol simultaneously acted as a solvent and a reductant, while water served only as a cosolvent. The abundant oxygen-containing functional groups of graphene oxide played extremely important roles in the growth of Ru nanoparticles on the resultant graphene nanosheets, as they promoted Ru nucleation and acted as anchor sites for the Ru nanoparticles. Moreover, the use of water as a cosolvent was an effective way to tune the Ru particle size and morphology and aid in the loading of the nanocomposite, resulting in dramatically enhanced catalytic activity in comparison with a composite prepared by using ethylene glycol as a single solvent (SS-Ru/graphene). The exceptional catalytic performance of the CS-Ru/graphene was mainly ascribed to the novel graphene support that simultaneously combines a large specific surface area with excellent electronic conductivity, but also to the highly dispersive Ru nanoparticles that made up the nanocomposite with a controlled morphology and an optimal size.

Introduction

There is an ever-growing demand to use hydrogen instead of fossil fuels to deal with energy shortage issues and to reduce carbon dioxide emissions; however, the extremely low volumetric density of gaseous hydrogen significantly hinders the use of hydrogen.^{1,2} Using ammonia as a hydrogen carrier is a promising and feasible solution to facilitate hydrogen storage and transportation, in terms of its attractive hydrogen storage capacity under mild conditions as well as the existence of a well-established infrastructure.^{3–7} Therefore, for an ammonia-mediated hydrogen economy, the effective release of hydrogen from ammonia *via* catalytic decomposition is of great importance for practical hydrogen utilization. A great deal of effort has been dedicated to exploring high-performance catalysts in the past, and various metal catalysts including Ru,^{8–23} Fe,^{14,16, 24–28} Co,^{14,28} Ni,^{16,29–31} Pt,^{16,32} and Pd^{14,16} *etc.* have been widely examined for use in ammonia decomposition. The activities of various metals are well correlated with the binding energy of nitrogen atoms to the metal catalysts, following a volcano-type relationship.^{4,33} As a result of the optimal heat of nitrogen chemisorptions,³³ Ru has

proven to be the most active among various single-metal catalysts for ammonia decomposition. Consequently, Ru-based catalysts have attracted particular attention for hydrogen production from ammonia because of their excellent catalytic performance.

Experimental observations have revealed that the catalytic activity of Ru is support-dependant,^{5,15–17} that is, the catalytic performance of catalysts differs significantly according to the type of support used. Yin *et al.*¹⁰ conducted a comparative study of various kinds of supported Ru catalysts for ammonia decomposition. They concluded that Ru supported by carbon nanotubes (CNTs) showed the highest catalytic performance mainly related to the high Ru dispersion on CNTs, and to the high graphitization and high purity of CNT materials. In another study, Li and coworkers¹⁷ observed that the catalytic activity of Ru differed greatly when using different types of carbon supports. Graphite carbon-supported Ru showed the best catalytic performance, although Ru dispersion on the graphite carbon was not the best. It is believed that the nature of the support exerts a very important influence on the catalytic activity of Ru in ammonia decomposition. On the other hand, as a result of the variation in the abundance of highly active B₅-type sites for

different Ru structures,^{18–20} ammonia decomposition with Ru is known to be a structure-sensitive reaction. Several groups^{8,20,21} have reported the strong effect of Ru particle size on Ru catalytic activity. More recently, Karim *et al.*¹¹ conducted an experimental and theoretical study and determined that the catalytic activity of Ru was dependent not only on Ru particle size, but also on Ru particle shape. Based on the unique features of support dependence and structure sensitivity of Ru activity in ammonia decomposition, the hybridization of a novel support and Ru nanoparticles with a well-controlled size and morphology would reasonably result in an advanced catalyst, which is of vital practical importance in producing CO_x-free hydrogen from ammonia.

Graphene is a two-dimensional atomically thick carbon sheet, which has recently garnered tremendous scientific and technical interest for various applications as a result of its fascinating electrical, optical, mechanical and thermal properties.^{34–36} Typically, graphene decorated with metals or metallic compounds may lead to a variety of advanced hybrid materials with unusual properties,^{37,38} which provides a very feasible and effective route to a significant expansion of the application of graphene material. When its relatively large specific surface area is taken into account, graphene would also be a very interesting two-dimensional nanomaterial as a support for anchoring Ru nanoparticles in catalysis.

In the present study, we report the *in-situ* growth of Ru nanoparticles on graphene nanosheets by reducing a solution of graphene oxide and RuCl₃ to form a Ru/graphene nanocomposite as a catalyst for ammonia decomposition. In the composite preparation, ethylene glycol simultaneously acted as a solvent and a reducing agent. The multiple functions of graphene oxide, the precursor of graphene, were expected to be an asset to the nanoarchitecture of the composite. In this work, we compared a nanocomposite (CS-Ru/graphene) that derived from a cosolvent (water) method with the other one (SS-Ru/graphene) that derived from a single solvent (ethylene glycol) method, and demonstrated a dramatically enhanced nanoarchitecture for the nanocomposite version with respect to Ru particle size, morphology and loading, which resulted in greatly enhanced catalytic activity. Results from the present study showed that this novel CS-Ru/graphene composite can be used as a highly efficient and promising catalyst for CO_x-free hydrogen production from ammonia.

Experimental

Materials

Natural graphite flakes (>99.8%, 325 mesh) were purchased from Alfa Aesar. RuCl₃·nH₂O and ethylene glycol were purchased from Wako Pure Chemical Industries, Ltd., Japan. KMnO₄, concentrated H₂SO₄ (98%), and H₂O₂ were purchased from Sigma-Aldrich. All chemicals were used as received.

Preparation of CS-Ru/graphene and SS-Ru/graphene

Graphite oxide was prepared according to a previously reported procedure.³⁹ First, 4 mg graphite oxide was dissolved in an 80 g water-ethylene glycol (volume ratio=1/1) mixture, and the graphite oxide solution was then subjected to sonication treatment at 28 kHz in a VS-100III bath-type sonicator (Iuchi Seieido, Osaka, Japan) for 1 h to obtain graphene oxide. Subsequently,

60 mg RuCl₃·nH₂O was added into the graphene oxide solution, and was stirred for 30 min at room temperature to form a homogenous solution. After sonication for another 1 h, the mixture was transferred to a Teflon-lined autoclave and heated at 200 °C under autogenous pressure for 3 h. The obtained solid product was then filtered and washed with water, and this procedure was repeated 5 times. Finally, the CS-Ru/graphene nanocomposite was obtained after it was vacuum dried at 60 °C overnight. SS-Ru/graphene nanocomposite was prepared using the same procedure with the exception of using equal volume of pure ethylene glycol instead of a water-ethylene glycol mixture during synthesis.

Characterization

X-ray photoelectron spectroscopy (XPS) analyses were carried out using a JPS-90MS photoelectron spectrometer (JEOL, Japan) with Mg K α radiation (hv=1253.6 eV) in a vacuum of < 10⁻⁷ Pa. Powder X-ray diffraction (XRD) patterns were recorded on a D/Max-2500 X-ray diffractometer (Rigaku, Japan) with Cu K α radiation (λ =1.54056 Å) at a scan rate of 0.05° s⁻¹. Fourier transform infrared spectroscopy (FT-IR) spectra were collected with samples deposited on a KBr plate using a FT/IR-4100 spectrophotometer (Jasco, Japan) and wavenumbers that ranged from 1,000–4,000 cm⁻¹. Raman spectra were required on a NRS-5100 Raman spectrometer (Jasco, Japan) with an excitation laser of 532 nm. Atomic force microscopy (AFM) images were taken using Nanocute scanning probe microscopy (SII Nanotechnology Inc., Japan) operated under a tapping model. Scanning electron microscope (SEM) images were taken on a JCM-5700 SEM (JEOL, Japan) using an accelerating voltage of 20 kV. Transmission electron microscope (TEM) images, selected area electron diffraction (SAED) patterns and energy dispersive X-ray spectroscopy (EDX) analyses were obtained on a JEM-2011 TEM (JEOL, Japan) using an accelerating voltage of 200 kV. Thermogravimetric analysis (TGA) and differential thermal analysis (DTA) were simultaneously performed on a DTG-60 instrument (Shimadzu, Japan) at a heating rate of 10 °C min⁻¹ under He and air atmospheres, respectively. The interaction between Ru nanoparticles and graphene nanosheets was examined by sonicating a water dispersion of CS-Ru/graphene (0.05 g ml⁻¹) at 28 kHz for 30 min using a VS-100III bath-type sonicator (Iuchi Seieido, Osaka, Japan) under room temperature. Particle size distributions (PSDs) of Ru on graphene sheets were estimated by measuring a randomly selected area with more than 150 particles for each sample.

Catalyst testing

The catalytic activities of the CS-Ru/graphene and SS-Ru/graphene nanocomposites were evaluated in a quartz tube, fixed-bed reactor with an inner diameter of 6 mm under atmospheric pressure, with 50 mg of the catalysts loaded in the reactor. Prior to the measurement, the reactor was purged with He under a flow rate of 100 ml min⁻¹ for 30 min. The reactor was then heated to desired test temperatures of 350–500 °C, and pure ammonia was then fed into the reactor at a GHSV of 20,000 or 30,000 ml h⁻¹ g_{cat}⁻¹. Gas compositions from the reactor were analyzed by GC-14B gas chromatography (Shimadzu, Japan) equipped with a thermal conductor and a Porapak N column using N₂ as a carrier gas.

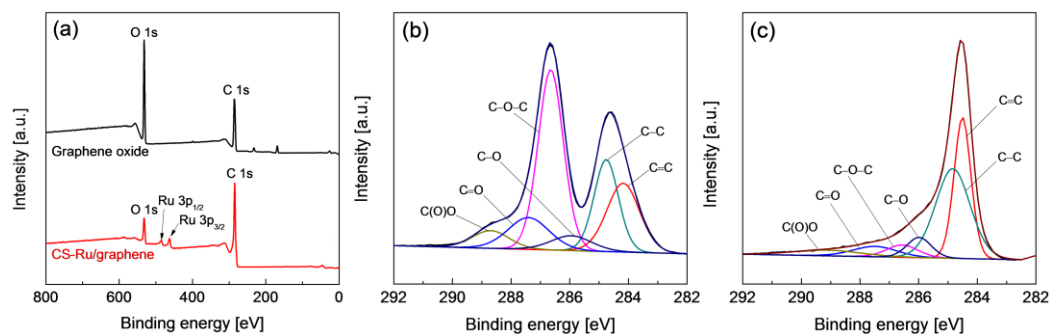


Figure 1. (a) Survey XPS spectra of graphene oxide and CS-Ru/graphene. (b) High-resolution C 1s XPS spectra of graphene oxide. (c) High-resolution C 1s XPS spectra of CS-Ru/graphene.

5

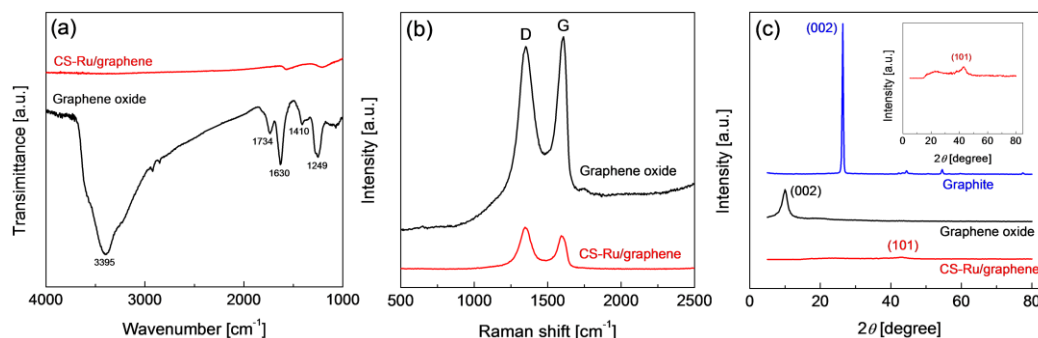


Figure 2. (a) FT-IR spectra of graphene oxide and CS-Ru/graphene. (b) Raman spectra of graphene oxide and CS-Ru/graphene. (c) XRD patterns of graphite flakes, graphene oxide and CS-Ru/graphene. The insert in (c) shows magnified XRD pattern of CS-Ru/graphene.

Results and discussion

10 Characterization of CS-Ru/graphene nanocomposites

Figure 1a shows a survey of the XPS spectra of graphene oxide and a CS-Ru/graphene nanocomposite. Both graphene oxide and CS-Ru/graphene showed obvious peaks centered at the binding energies of around 532.1 and 286.1 eV, which were assigned to O 1s and C 1s XPS signals, respectively. For the CS-Ru/graphene, however, additional peaks centered at the binding energies of 485.08 and 463.36 eV were observed, which were assigned to Ru 3p_{1/2} and Ru 3p_{3/2} peaks, respectively, indicating the formation of a composite containing C, O, and Ru elements after the simultaneous reduction of graphene oxide and RuCl₃ in the water-ethylene glycol system. These results agreed well with those found by an EDX measurement (Figure S1). Figures 1b and 1c clearly show the evolution of the chemical surroundings of carbon during the reduction process. The C 1s XPS peaks were deconvoluted into the following components: sp² carbon C=C and sp³ carbon C—C in aromatic rings, and oxygenated carbon including hydroxyl carbon C—O, epoxy carbon C—O—C, carbonyl carbon C=O, and carboxyl carbon C(O)O.⁴⁰ Apart from the C=C (284.2 eV) and C—C (284.8 eV), the C 1s XPS of graphene oxide consisted of C—O—C (286.6 eV) with a very high intensity, together with considerable C—O (286.0 eV), C=O (287.4 eV) and C(O)O (288.7 eV) components, indicating abundant oxygen-containing functional groups in the graphene oxide. However, the peak intensities of those oxygen containing

35 groups were greatly decreased in the CS-Ru/graphene, particularly for the C—O—C peak. This result shows that most of the oxygen-containing groups had been removed after the reduction process for the graphene in the CS-Ru/graphene, confirming a very effective reduction process.

40 To further study the structural changes during the chemical reduction process, both graphene oxide and the CS-Ru/graphene composite were characterized by FT-IR and Raman spectroscopy. Figure 2a shows the FT-IR spectra of graphene oxide and CS-Ru/graphene. Graphene oxide showed the main absorption bands at 3395, 1734, 1410, 1249, and 1052 cm⁻¹, which were assigned to O—H stretching, C=O stretching, O—H deformation, C—O—C stretching, and C—O stretching vibrations,⁴¹ respectively. However, those peaks nearly disappeared for CS-Ru/graphene, indicating an effective reduction reaction on graphene had occurred. Raman spectroscopy is a useful and effective technique to gain insight into the structure of carbon materials. The D band centered at ~1350 cm⁻¹ in the spectra was assigned to the breathing mode of the κ-point phonons of A_{1g} symmetry, while the G band centered at ~1580 cm⁻¹ corresponds to the E_{2g} phonons of sp² carbon atoms.⁴² Therefore, the intensity ratio of the D to G (I_D/I_G) band was used as a measure of the degree of disorder and the crystalline size of the carbon materials. Figure 2b shows the Raman spectra of the graphene oxide and the CS-Ru/graphene nanocomposite. The I_D/I_G of CS-Ru/graphene (1.28) was increased compared with that of graphene oxide (0.95), which could be ascribed to a decrease in the average size of sp² domains for graphene oxide after reduction.⁴² Moreover, the

intensities of both D and G bands for CS-Ru/graphene were lower than those in graphene oxide, suggesting the deposition of Ru particles with a high loading in CS-Ru/graphene. These results provide further support to confirm the effective reduction of both Ru³⁺ ions and graphene oxide.

Figure 2c compares the XRD patterns of graphite flakes, graphene oxide and CS-Ru/graphene. The graphite flakes showed a strong (002) diffraction peak at $2\theta=26.5^\circ$, corresponding to a d -spacing of 0.34 nm. After the graphite flakes were oxidized to graphene oxide, the (002) peak was shifted to a lower angle of $2\theta=10.2^\circ$, which corresponded to a significantly enlarged d -spacing of 0.87 nm. This increased interlayer distance of the graphene oxide could be ascribed to the embedding of a considerable amount of oxygen-containing functional groups and intercalation of water molecules in the graphitic layers.^{43,44} In the CS-Ru/graphene, the (002) diffraction peak disappeared, which indicated a disorder of the regular stacking of the original graphitic layers,⁴⁵ and further confirmed the formation of single- or/and few-layer graphene nanosheets. Moreover, an additional diffraction peak at $2\theta=43.0^\circ$ was observed, which could be assigned to the (101) Ru crystallographic planes. The highly broadened diffraction peak of Ru showed the formation of nanosized Ru particles on graphene nanosheets. The deposition of Ru nanoparticles was expected to effectively prevent the restacking of graphene nanosheets after the reduction process. AFM observation confirmed that the as-prepared CS-Ru/graphene was around 3 nm in thickness (Figure S2).

The bulk CS-Ru/graphene nanocomposite had a sponge-type architecture with an average pore size of several micrometers (Figure S3). This porous structure was most likely generated by the rapid evaporation of water from the as-obtained composite during the vacuum drying process, which effectively avoided the aggregation of CS-Ru/graphene and enabled more exposure of the active surface area that was readily accessible for guest molecules in catalysis. The TEM images of CS-Ru/graphene with different magnifications shown in Figures 3a and 3b demonstrate

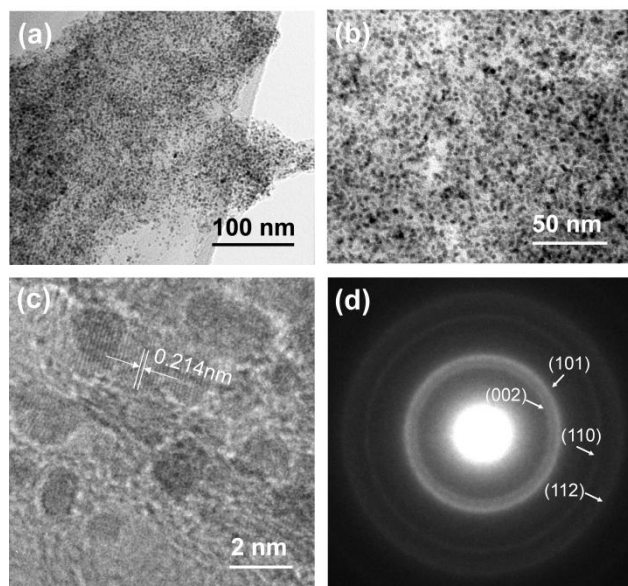


Figure 3. (a, b) TEM images of the CS-Ru/graphene at different magnifications. (c) High-resolution TEM image of CS-Ru/graphene. (d) SAED patterns of CS-Ru/graphene.

that Ru nanoparticles were homogeneously deposited onto the surface of graphene nanosheets, and had a rather small PSD in the composite (Figure S4a). The high-resolution TEM image in Figure 3c shows the deposited Ru particles were spherical-shaped with an average size of 2.2 nm, and the d -spacing obtained from the lattice fringes was 0.214 nm, which was consistent with the d -spacing value of the (002) crystallographic planes of the metallic Ru, confirming the successful deposition of Ru nanoparticles on the graphene nanosheets. Moreover, the SAED patterns (Figure 3d) of the CS-Ru/graphene showed a polycrystalline structure as a result of the growth of nanosized Ru particles in the composite. The measured d -spacing for different crystallographic planes from the SAED patterns were 0.214, 0.205, 0.135, and 0.143 nm, which was consistent with the d -spacing values of (002), (101), (110), and (112) crystallographic planes of the hexagonal Ru crystals obtained by XRD (JCPDS card No.: 6-663), and provided further evidence supporting the growth of the Ru nanoparticles on the graphene nanosheets.

Roles of graphene oxide and cosolvent in the nanocomposite formation

To gain insight into the function of graphene oxide in the hybridization process of CS-Ru/graphene, Ru particles were prepared without graphene oxide in the synthesis solution while other reaction conditions were identical. It is interesting that the obtained Ru particles easily precipitated in ethylene glycol, showing a very large particle size (Figure S5). Obviously, the presence of graphene oxide exerted a very strong influence on the formation of Ru nanoparticles. As confirmed in the aforementioned discussion concerning the XPS (Figure 1) and FT-IR (Figure 2a) results, graphene oxide possessed abundant oxygen-containing functional constituents, such as hydroxyl and epoxy, which made the graphene oxide nanosheets highly hydrophilic and easily dispersed in a water-ethylene glycol homogeneous mixture. On the other hand, these functional groups promoted metal nucleation and acted as anchoring sites for the deposition of metal nanoparticles.^{35,46,47} As a result, a great amount of Ru nuclei were uniformly generated on the homogeneously dispersed graphene oxide in the synthesis solution, resulting in highly dispersed Ru nanoparticles on graphene nanosheets with an extremely narrow PSD after the subsequent growth of Ru nuclei. Moreover, Ru nuclei seemed to preferentially form on the graphene oxide nanosheets rather than in the liquid phase. This was supported by the fact that the amount of Ru crystals in the Ru/graphene nanocomposite was significantly higher than it was in the liquid phase. These results led us to believe that Ru³⁺ ions were possibly first absorbed by the oxygen-containing groups, which facilitated Ru nucleation onto the graphene oxide during the initial reduction process, and finally resulted in a CS-Ru/graphene nanocomposite after the growth of Ru nuclei along with deoxygenation of the graphene oxide.

Note that the strong interaction between Ru and the support played a very important role in the successful obtainment of a high-quality Ru/graphene nanocomposite, because it immobilized the Ru nuclei and the resultant nanoparticles, and thereby prevented the agglomeration that generally leads to large particles during synthesis. As observed in the system in the absence of graphene oxide (Figure S5), the size of prepared Ru particles

reached several hundred nanometers, and probably suffered from a serious agglomeration effect during synthesis. To avoid this phenomenon, a polymer surfactant (*e.g.*, polyvinylpyrrolidone) was usually added in the liquid polyol as a stabilizer in the polyol method.^{48,49} However, the adsorbed thin polymer layer on the Ru particle surface was found to significantly affect its catalytic performance in an adverse manner.⁴⁹ In the present system, Ru nanoparticles stabilized by a novel two-dimensional nanomaterial using no polymer surfactant seemed to be advantageous for catalysis. Obviously, apart from providing a novel two-dimensional catalyst support, the multifunctional graphene oxide also drastically promoted Ru nucleation and effectively served as a new stabilizer to prevent the agglomeration of the Ru nuclei and nanoparticles.

The polyol method is a very effective way to prepare Ru nanoparticles. The addition of water as a solvent in the synthesis solution is seldom applied in the reported work, because the liquid polyol (*e.g.*, ethylene glycol) simultaneously acts as both a solvent and a reductant in this method. Thus, an anhydrous system is usually used.^{48,49} Although both graphene oxide and RuCl₃ are soluble in ethylene glycol, considering the highly hydrophilic properties of graphene oxide and its significant roles in the Ru nanoparticle formation process, the effect of water as a cosolvent in the precursor solution must be examined in an attempt to improve the nanostructure of the composite. In comparison with SS-Ru/graphene prepared without water as a cosolvent, using water as a cosolvent was of great importance in the obtaining of a high-quality nanocomposite. When the system was free of water, and ethylene glycol acted as a single solvent for the dispersion of graphene oxide in the reduction process, the SS-Ru/graphene showed poor quality compared with CS-Ru/graphene. As shown in Figure 4, in sharp contrast, the Ru particles were completely morphologically different and irregularly shaped in the composite. Moreover, Ru particles grown on the graphene nanosheets showed a much larger average size (15.2 nm (Figure S4b)), and the Ru loading density was significantly decreased. This was probably due to fewer Ru nuclei being generated on the graphene oxide during the nucleation step. The use of water as a cosolvent in this work definitely helped control the preparation process with regard to Ru size, morphology and loading in the composite. The addition of a cosolvent may have enhanced graphene oxide dispersion and promoted Ru nucleation because of the excellent affinity between the highly hydrophilic graphene oxide and water. Moreover, water-ethylene glycol as the growth media may affect the growth of Ru nuclei in the cosolvent system, leading to more isotropic Ru nanoparticles. Therefore, this cosolvent system successfully

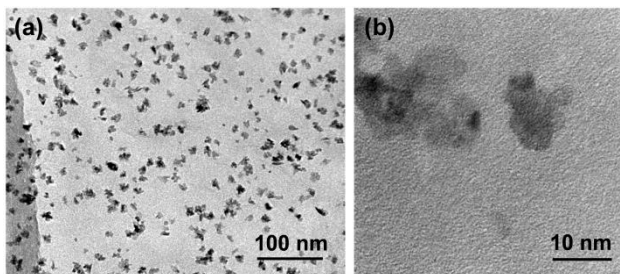


Figure 4. TEM images of SS-Ru/graphene with different magnifications prepared without water as a cosolvent.

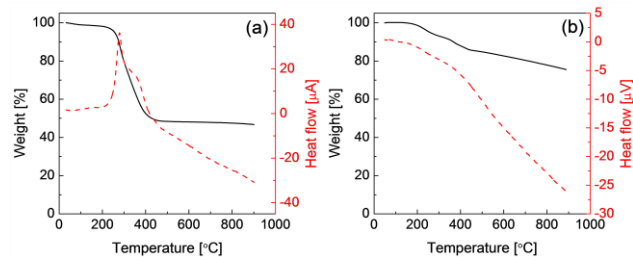


Figure 5. TGA/DTA curves of CS-Ru/graphene in an air (a) and in a He (b) atmosphere.

allowed the control of both Ru nucleation and growth on graphene nanosheets during synthesis, eventually resulting in an improved nanoarchitecture in the composite. Additionally, the cosolvent system could effectively reduce the consumption of organic solvent during synthesis, which made the preparation process more environmentally friendly.

Catalytic activity and stability

Figures 5a and 5b show the TGA/DTA curves of a CS-Ru/graphene nanocomposite under air and He atmospheres, respectively. Under an air atmosphere, the weight of CS-Ru/graphene gradually decreased as the temperature was increased to 250 °C. This could be mainly assigned to the removal of adsorbed water molecules. A significant weight loss was then observed at temperatures ranging from 250 to 400 °C, accompanying a strong heat release, as a result of the complete combustion of graphene nanosheets with oxygen. No apparent weight loss was detected when the temperature was higher than 400 °C. The Ru loading was estimated to be 35 wt% in the composite, which assumed the residue was in the form of RuO₂ after oxidation at 900 °C. When the measurement was carried out under a He atmosphere, the weight of the CS-Ru/graphene gradually decreased as the temperature was increased to 900 °C, mainly due to the removal of adsorbed water molecules and surface oxygen-containing functional groups on the graphene nanosheets. The total weight loss was only 25 wt% at 900 °C under a He atmosphere, which was much less than the 53 wt% under an air atmosphere, indicating that the composite was more stable under an oxygen-free atmosphere at high temperatures. Sonication treatment was used to further study the stability of CS-Ru/graphene in terms of the binding force between the Ru nanoparticles and the graphene nanosheets in the composite. There was no very apparent change, neither in the Ru dispersion nor in the loading amount in the CS-Ru/graphene, regardless of the treatment (Figure S6), which indicated that in the chemically converted CS-Ru/graphene, the Ru nanoparticles had formed a strong covalent bond to the basal plane of the graphene nanosheets.⁴⁶ These results show that CS-Ru/graphene has the potential to be a high-temperature stable catalyst for practical applications. The durability of the CS-Ru/graphene catalyst in ammonia decomposition was tested for the catalytic decomposition of ammonia at 450 °C for a period of 110 h. As shown in Figure 6, ammonia conversion was almost constant, indicating a very stable catalytic performance at a high temperature.

Figure 7 shows the temperature dependence of CS-

Table 1. Comparison of the catalytic performance of CS-Ru/graphene with several typical Ru-based ammonia decomposition catalyst at GHSV=30,000 ml h⁻¹ g_{cat}⁻¹.

Catalyst	Temperature [°C]	H ₂ production rate [mmol min ⁻¹ g _{cat} ⁻¹]	Conversion [%]	Reference
Ru/Al ₂ O ₃	450	1.9	5.9	[10]
Ru/MCM-41	450	14.2	42.4	[22]
Ru/SBA-15	450	16.4	49.0	[22]
Ru/SiO ₂	450	11.4	36.4	[23]
Ru/CMK-3	550	7.0	22.7	[9]
Ru/activated carbon	550	4.4	14.4	[17]
Ru/CNTs	550	26.0	84.7	[17]
Ru/CNTs	500	28.35	84.65	[16]
Ru/CNTs	450	14.6	43.7	[13]
K-Ru/CNTs	450	32.6	97.3	[13]
CS-Ru/graphene	450	28.7	85.8	This study

Ru/graphene and SS-Ru/graphene catalysts during ammonia decomposition. With increasing temperature, the ammonia conversion increased rapidly for both catalysts, mainly due to the improved reaction rate at high temperatures. However, within the entire temperature range, because of the significantly improved nanoarchitecture, the CS-Ru/graphene obtained *via* a cosolvent method showed a much higher ammonia conversion compared with that of SS-Ru/graphene prepared using a single-solvent method. For comparison, Table 1 summarizes the catalytic performance of CS-Ru/graphene and other typical Ru-based catalysts reported previously for ammonia decomposition. Note that CS-Ru/graphene showed ammonia conversion of 85.8%, corresponding a high hydrogen production rate of 28.7 mmol min⁻¹ g_{cat}⁻¹, at GHSV=30,000 ml h⁻¹ g_{cat}⁻¹ and 450 °C, which far exceeded the normal conversions of 5~50% for other supported Ru catalysts reported in the literature under the same conditions or even much higher reaction temperatures, which indicates that Ru supported by the two-dimensional graphene nanosheets was a very effective catalyst for ammonia decomposition. Previously, Ru supported by CNTs (Ru/CNTs) was considered to be a high-performance catalyst for ammonia decomposition.^{10,13,16} However, the CS-Ru/graphene composite definitely showed much better catalytic performance. Although the catalytic activity of

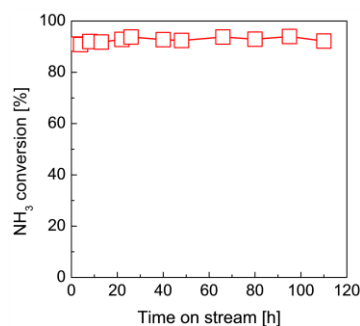


Figure 6. Time course of ammonia decomposition at 450 °C using CS-Ru/graphene as a catalyst. GHSV=20,000 ml h⁻¹ g_{cat}⁻¹.

Ru/CNTs could be significantly enhanced with the increased basicity of the support with an alkali promoter (*e.g.*, K-Ru/CNTs),⁵ the catalytic performance of CS-Ru/graphene seemed comparable even without the addition of a promoter. Moreover, it is noteworthy that the cost of graphene nanosheets in large-scale production are estimated to be much lower than that of CNTs,³⁴ which confers a great advantage to graphene nanosheets over the use of CNTs in support of Ru catalysts for CO_x-free hydrogen production from ammonia on an industrial scale.

We believe this new two-dimensional graphene support plays a very important role in obtaining high catalytic performance for Ru crystals. First, compared with other supports, graphene nanosheets have an extremely large specific surface area, which is advantageous to the loading of highly dispersive Ru nanocrystals, resulting in the exposure of a considerable amount of active sites for catalytic reaction. On the other hand, the recombination of nitrogen atoms is generally regarded as the rate-determining step in ammonia decomposition.^{8,16,25,50} An electronic conductive support can facilitate electron transfer from a support to Ru, which is thought to favor the recombinative desorption of nitrogen atoms and results in enhanced catalytic activity.⁵ The excellent conductivity of graphene, therefore,

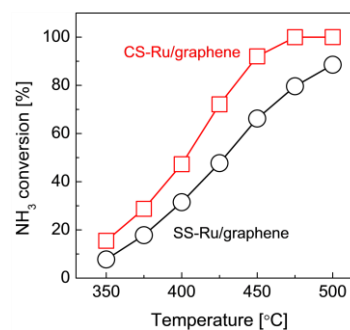


Figure 7. Temperature dependence of ammonia decomposition using CS-Ru/graphene and SS-Ru/graphene as catalysts. GHSV=20,000 ml h⁻¹ g_{cat}⁻¹.

would make another crucial contribution to the high catalytic performance of the CS-Ru/graphene catalyst. Additionally, because the ammonia decomposition performance is effectively affected by the Ru particle size and morphology,¹¹ and the optimal average particle size that will allow the highest turnover frequency for spherical-shaped Ru nanoparticles reportedly ranges from 1.8~2.5 nm.^{11,18} In the present work, the cosolvent method enabled the growth of Ru nanocrystals with a controlled spherical morphology and an optimal size of 2.2 nm, which would also further enhance the catalytic activity of Ru in the nanocomposite.

In summary, we show that Ru nanoparticles supported by two-dimensional graphene nanosheets had easily controllable morphology, size and loading *via* a cosolvent method, and they exhibited both excellent stability and greatly improved catalytic activity for ammonia decomposition. These nanocomposites demonstrated great potential as an alternative catalyst for practical CO_x-free hydrogen production from ammonia.

Conclusions

A high-quality CS-Ru/graphene nanocomposite was obtained *via* the *in-situ* growth of Ru nanoparticles on graphene nanosheets using a cosolvent method, and was applied as a catalyst to produce CO_x-free hydrogen from ammonia. The mass number of oxygen-containing functional groups on the graphene oxide significantly promoted Ru nucleation on the support and effectively prevented the aggregation of the Ru nuclei during synthesis. When compared with an anhydrous synthesis system, the utilization of water as a cosolvent during synthesis helped to control the Ru particle size and morphology as well as its loading into the nanocomposite. In constructing the CS-Ru/graphene nanocomposite, spherical-shaped Ru nanocrystals were homogeneously grown on the graphene nanosheets to an average particle size of 2.2 nm with loading that reached as high as 35 wt%. Ammonia was almost completely decomposed at 475 °C with a GHSV of 20,000 ml g_{cat}⁻¹ min⁻¹, and the catalyst showed stable catalytic performance at 450 °C for a period of 110 h. Compared with other catalyst supports, when graphene nanosheets were used to support Ru nanoparticles, catalytic performance was improved significantly as a result of the high specific surface area and good electronic conductivity combined with excellent control of the Ru particle size, morphology and loading when using the cosolvent method. This CS-Ru/graphene-nanocomposite with improved nanoarchitecture, excellent catalytic activity, and durability is a very promising catalyst for CO_x-free hydrogen production from ammonia.

Notes and references

^a School of Light Industry & Food Science, South China University of Technology, No. 381 Wushan Road, Guangzhou, China.

^b Department of Chemical Engineering, Hiroshima University, 1-4-1

Kagamiyama, Higashi-Hiroshima, Japan. Fax: +81 82 4245494; Tel: +81 82 4247714; E-mail: tsuru@hiroshima-u.ac.jp

† Electronic Supplementary Information (ESI) available: [Details regarding EDX, AFM, SEM, TEM, and PSD of the CS-Ru/graphene, PSD of the SS-Ru/graphene, and TEM image of Ru particles prepared in the absence of graphene oxide]. See DOI: 10.1039/b000000x/

1 L. Schlapbach and A. Züttel, *Nature*, 2001, **414**, 353.

- 2 B. Sakintuna, F. Lamari-Darkrim and M. Hirscher, *Int. J. Hydrogen Energy*, 2007, **32**, 1121.
- 3 A. Klerke, C. H. Christensen, J. K. Nørskov and T. Vegge, *J. Mater. Chem.*, 2008, **18**, 2304.
- 4 F. Schüth, R. Palkovits, R. Schlögl and D. S. Su, *Energy Environ. Sci.*, 2012, **5**, 6278.
- 5 S. F. Yin, B. Q. Xu, W. P. Zhou and C. T. Au, *Appl. Catal. A*, 2004, **277**, 1.
- 6 G. Li, M. Kanezashi, T. Yoshioka and T. Tsuru, *AIChE J.*, 2013, **59**, 168.
- 7 C. H. Christensen, T. Johannessen, R. Z. Sørensen and J. K. Nørskov, *Catal. Today*, 2006, **111**, 140.
- 8 W. Zheng, J. Zhang, H. Xu and W. Li, *Catal. Lett.*, 2007, **119**, 311.
- 9 L. Li, Z. H. Zhu, G. Q. Lu, Z. F. Yan and S. Z. Qiao, *Carbon* **2007**, **45**, 11.
- 10 S. F. Yin, B. Q. Xu, W. X. Zhu, C. F. Ng, X. P. Zhou and C. T. Au, *Catal. Today*, 2004, **93–95**, 27.
- 11 A. M. Karim, V. Prasad, G. Mpourmpakis, W. W. Lonergan, A. I. Frenkel, J. G. Chen and D. G. Vlachos, *J. Am. Chem. Soc.*, 2009, **131**, 12230.
- 12 Y. Li, L. Yao, Y. Song, S. Liu, J. Zhao, W. Ji and C. T. Au, *Chem. Commun.*, 2010, **46**, 5298.
- 13 S. F. Yin, B. Q. Xu, C. F. Ng and C. T. Au, *Appl. Catal. B*, 2004, **48**, 237.
- 14 R. Z. Sørensen, L. J. E. Nielsen, S. Jensen, O. Hansen, T. Johannessen, U. Quaade and C. H. Christensen, *Catal. Commun.*, 2005, **6**, 229.
- 15 F. R. García-García, J. Álvarez-Rodríguez, I. Rodríguez-Ramosa and A. Guerrero-Ruizb, *Carbon*, 2010, **48**, 267.
- 16 S. F. Yin, Q. H. Zhang, B. Q. Xu, W. X. Zhu, C. F. Ng and C. T. Au, *J. Catal.*, 2004, **224**, 384.
- 17 L. Li, Z. H. Zhu, Z. F. Yan, G. Q. Lu and L. Rintoul, *Appl. Catal. A*, 2007, **320**, 166.
- 18 W. Raróg-Pilecka, E. Miśkiewicz, D. Szmigiel and Z. Kowalczyk, *J. Catal.*, 2005, **231**, 11.
- 19 C. J. H. Jacobsen, S. Dahl, P. L. Hansen, E. Törnqvist, L. Jensen, H. Topsøe, D. V. Prip, P. B. Møenshaug and I. Chorkendorff, *J. Mol. Catal. A: Chem.*, 2000, **163**, 19.
- 20 F. R. García-García, A. Guerrero-Ruiz and I. Rodríguez-Ramos, *Top. Catal.*, 2009, **52**, 758.
- 21 W. Raróg-Pilecka, D. Szmigiel, A. Komornicki, J. Zieliński and Z. Kowalczyk, *Carbon*, 2003, **41**, 589.
- 22 X. K. Li, W. J. Ji, J. Zhao, S. J. Wang and C. K. Au, *J. Catal.*, 2005, **236**, 181.
- 23 T. V. Choudhary, C. Sivadinarayana and D. W. Goodman, *Catal. Lett.*, 2001, **72**, 197.
- 24 M. Feyn, C. Weidenthaler, R. Güttel, K. Schlichte, U. Holle, A. H. Lu and F. Schüth, *Chem. Eur. J.*, 2011, **17**, 598.
- 25 L. Wang, Y. Zhao, C. Liu, W. Gong and H. Guo, *Chem. Commun.*, 2013, **49**, 3787.
- 26 A. H. Lu, J. J. Nitz, M. Comotti, C. Weidenthaler, K. Schlichte, C. W. Lehmann, O. Terasaki and F. Schüth, *J. Am. Chem. Soc.*, 2010, **132**, 14152.
- 27 X. Duan, G. Qian, X. Zhou, Z. Sui, D. Chen and W. Yuan, *Appl. Catal. B*, 2011, **101**, 189.
- 28 J. Zhang, M. Comotti, F. Schüth, R. Schlögl and D. S. Su, *Chem. Commun.*, 2007, 1916.
- 29 J. Zhang, H. Xu and W. Li, *Appl. Catal. A*, 2005, **296**, 257.
- 30 J. Ji, X. Duan, G. Qian, X. Zhou, D. Chen and W. Yuan, *Ind. Eng. Chem. Res.*, 2013, **52**, 1854.
- 31 Q. F. Deng, H. Zhang, X. X. Hou, T. Z. Ren and Z. Y. Yuan, *Int. J. Hydrogen Energy*, 2012, **37**, 15901.
- 32 W. Tsai, J. J. Vajo and W. H. Weinberg, *J. Phys. Chem.*, 1985, **89**, 4926.
- 33 D. A. Hansgen, D. G. Vlachos and J. G. Chen, *Nat. Chem.*, 2010, **2**, 484.
- 34 D. Li and R. B. Kaner, *Science*, 2008, **320**, 1170.
- 35 H. Bai, C. Li and G. Shi, *Adv. Mater.*, 2011, **23**, 1089.
- 36 C. N. R. Rao, A. K. Sood, K. S. Subrahmanyam and A. Govindaraj, *Angew. Chem. Int. Ed.*, 2009, **48**, 7752.
- 37 Y. Liang, Y. Li, H. Wang, J. Zhou, J. Wang, T. Regier and H. Dai, *Nat. Mater.*, 2011, **10**, 780.

- 38 Q. Xiang, J. Yu and M. Jaroniec, *J. Am. Chem. Soc.*, 2012, **134**, 6575.
- 39 A. Dimiev, D. V. Kosynkin, L. B. Alemany, P. Chaguine and J. M. Tour, *J. Am. Chem. Soc.*, 2012, **134**, 2815.
- 5 40 M. Y. Yen, C. C. Teng, M. C. Hsiao, P. I. Liu, W. P. Chuang, C. C. M. Ma, C. K. Hsieh, M. C. Tsai and C. H. Tsai, *J. Mater. Chem.*, 2011, **21**, 12880.
- 41 J. Zhang, H. Yang, G. Shen, P. Cheng, J. Zhang, S. Guo, *Chem. Commun.*, 2010, **46**, 1112.
- 10 42 F. Tuinstra and J. L. Koenig, *J. Chem. Phys.*, 1970, **53**, 1126.
- 43 V. Eswaraiah, K. Balasubramaniam and S. Ramaprabhu, *Nanoscale*, 2012, **4**, 1258.
- 44 D. Pan, S. Wang, B. Zhao, M. Wu, H. Zhang, Y. Wang and Z. Jiao, *Chem. Mater.*, 2009, **21**, 3136.
- 15 45 Q. Xiang, J. Yu and M. Jaroniec, *J. Phys. Chem. C.*, 2011, **115**, 7355.
- 46 B. F. Machado and P. Serp, *Catal. Sci. Technol.*, 2012, **2**, 54.
- 47 G. Goncalves, P. A. A. P. Marques, C. M. Granadeiro, H. I. S. Nogueira, M. K. Singh, J. Grácio, *Chem. Mater.*, 2009, **21**, 4796.
- 20 48 X. Yan, H. Liu and K. Y. Liew, *J. Mater. Chem.*, 2001, **11**, 3387.
- 49 M. Zawadzki and J. Okal, *Mater. Res. Bull.*, 2008, **43**, 3111.
- 50 E. Shustorovich, *Surf. Sci. Lett.*, 1991, **259**, L791.